Acta Biomaterialia 23 (2015) 1–10

Contents lists available at ScienceDirect

Acta Biomaterialia

journal homepage: www.elsevier.com/locate/actabiomat

The armored carapace of the boxfish

Wen Yang [a,1], Steven E. Naleway [a,*], Michael M. Porter [a,2], Marc A. Meyers [a,b,c], Joanna McKittrick [a,b]

[a] Materials Science and Engineering Program, University of California, San Diego, La Jolla, CA 92093-0411, USA
[b] Dept. of Mechanical and Aerospace Engineering, University of California, San Diego, La Jolla, CA 92093-0411, USA
[c] Dept. of Nanoengineering, University of California, San Diego, La Jolla, CA 92093-0411, USA

ARTICLE INFO

Article history:
Received 1 December 2014
Received in revised form 24 April 2015
Accepted 21 May 2015
Available online 28 May 2015

Keywords:
Boxfish
Scute
Carapace
Fracture mechanism
Bioinspired

ABSTRACT

The boxfish (*Lactoria cornuta*) has a carapace consisting of dermal scutes with a highly mineralized surface plate and a compliant collagen base. This carapace must provide effective protection against predators as it comes at the high cost of reduced mobility and speed. The mineralized hydroxyapatite plates, predominantly hexagonal in shape, are reinforced with raised struts that extend from the center toward the edges of each scute. Below the mineralized plates are non-mineralized collagen fibers arranged in through-the-thickness layers of ladder-like formations. At the interfaces between scutes, the mineralized plates form suture-like teeth structures below which the collagen fibers bridge the gap between neighboring scutes. These sutures are unlike most others as they have no bridging Sharpey's fibers and appear to add little mechanical strength to the overall carapace. It is proposed that the sutured interface either allows for accommodation of the changing pressures of the boxfish's ocean habitat or growth, which occurs without molting or shedding. In both tension and punch testing the mineralized sutures remain relatively intact while most failures occur within the collagen fibers, allowing for the individual scutes to maintain their integrity. This complex structure allows for elevated strength of the carapace through an increase in the stressed area when attacked by predators in both penetrating and crushing modes.

1. Introduction

Many fish, reptiles (e.g. turtle and alligators) [1–5] and mammals (e.g. pangolin and armadillo [6]) have developed dermal armor for the same purpose of defending against the crushing and piercing attacks of predators. While almost all of these armors have developed with similar structures, they are implemented in different ways. One such example is the variety of connection methods between armor plates. These include the overlapping and articulating nature of fish scales [1–4], the non-mineralized collagen fibers (Sharpey's fibers) of armadillo osteoderms [6], the interlocking joints of the bony plates in seahorse armor [5,7,8], and the sutures of leatherback sea turtle scutes [2,3].

Within fish, the scales of the Senegal bichir [1] and alligator gar [4] are prime examples of ganoid scales, which provide protection through articulated arrays of tough bony plates covered by an enamel-like layer. On the other hand, elasmoid scales, such as those found in the arapaima [9,10], bass [11–13], carp [15], and sea bream [14,16] are more flexible with a greater degree of imbrication (overlap). They are also thinner and more flexible than the ganoid scales. Such scales contribute typically to less than 20% of the weight of fish while retaining mobility. In the arapaima and sea bass [9–12], the hardness decreases through the thickness of the scale toward the inside surface [9]. In addition to the mechanical properties of the fish scale layers, there are specific design qualities that dictate the ability of scales to provide protection while still allowing mobility and minimizing weight. These include the amount of overlap or imbrication, the ratio of the scale length to thickness, and the ratio of the scale length to the overall fish length. Fish scales from modern teleost fish are high-performance materials made of cross-plies of collagen type I fibrils reinforced with hydroxyapatite.

Recent studies on this material have demonstrated its remarkable performance in tension and against sharp puncture. The effect of tooth (or a tooth-like indenter) penetration on the scales was recently investigated by Song et al. [17] (for Senegal bichir (*Polypterus senegalus*)), Meyers et al. [9] (for arapaima (*Arapaimas gigas*)), and Zhu et al. [12,13] (for striped sea bass (*Morone saxatilis*)), who identified specific mechanisms. It was shown by Yang et al. [18] that it is difficult for a crack to advance in arapaima scales. A new fracture test setup where the scale is clamped between two pairs of miniature steel plates was developed by Dastjerdi and Barhtelat [19]. By preventing warping of the scales,

* Corresponding author. Tel.: +1 541 255 9998; fax: +1 858 534 5698.
E-mail address: snaleway@eng.ucsd.edu (S.E. Naleway).
[1] Address: ETH Zürich, Vladimir-Prelong-Weg 5, 8093 Zürich, Switzerland.
[2] Address: Department of Mechanical Engineering, Clemson University, Clemson, SC 29634, USA.

http://dx.doi.org/10.1016/j.actbio.2015.05.024
1742-7061/

they ensured controlled crack propagation. The work of fracture varied between 15 and 18 kJ/m^2 making teleost fish scales one of the toughest biological materials known.

In contrast to these flexible protective layers, the family of Ostraciidae has a rigid carapace [20,21]. Ostraciidae are members of the Tetraodontiformes order [22] that also includes pufferfish, porcupinefish, triggerfish, trunkfish, and ocean sunfish (e.g. Mola Mola) [23]. While the Tetraodontiformes employ many different defensive mechanisms, Ostraciidae are characterized by their boxy appearance (leading to their common name "boxfish") with a carapace composed of rigid scutes (or plates). The boxy shape and rigid carapace considerably restrict the movement of boxfish. Of note, this structure has led to extensive fluid dynamics studies as the unusual shape of the boxfish body and the placement of its fins create a number of vortices around the body and result in a sophisticated self-correcting swimming motion [24–29]. While a model for underwater locomotion, the boxfish is only capable of relatively slow swimming speeds of just above five body lengths per second [30]. Regardless, Ostraciidae have thrived for over 35 million years with effectively the same dermal armor [22].

As a characteristic example of the Ostraciidae armor, the scutes of the boxfish form a biocomposite composed of two basic constituents: mineral and protein. The mineralized component of the scutes is hydroxyapatite ($Ca_{10}(PO_4)_6(OH)_2$) and the organic constituent is mainly type I collagen, as found in other fish scales [1,4,14,21,31]. The structure of these scutes has been previously described by Besseau and Bouligand [21] who reported that the boxfish primarily has rigid hexagonal scutes formed through helical stacking (a Bouligand structure) of mineralized collagen supporting a mineralized plate. However, there is a current lack of literature related to the mechanical behavior of these scutes and how they might protect the boxfish from predation. Given the success of the boxfish in its natural environment, further understanding of these critical protective mechanics provides insight into bioinspired and materials research. Thus, the objective of this study is to correlate the structure, toughening mechanisms, and failure mechanics of the dermal armor of the boxfish.

2. Materials and methods

2.1. Boxfish samples

Four boxfish from two sources were used in this study. Three boxfish (*Lactoria cornuta*, catalog numbers SIO 14-20, SIO 95-125, SIO 95-141) were obtained from the Scripps Institution of Oceanography at the University of California (SIO), San Diego and preserved in a semi-dehydrated state in a 1:1 isopropanol (IPA) and water solution (Fig. 1(a)). These samples measured to be ~50 mm in length including the horns and tails (10–15 mm in length). One boxfish was purchased from Live Aquaria (2253 Air Park Road, WI, 54501, USA). This fish was shipped alive but died within a few days and was subsequently stored by freezing for two weeks (Fig. 1(b)). The external appearance of the fish from the two sources is similar. The fresh fish has a length approximately double that of the SIO preserved fish (~100 mm). The scutes are correspondingly larger for the 'fresh' fish: 8 mm vs. 5 mm (in diameter) for the preserved fish. The individual scutes were counted and categorized by shape (e.g. square, pentagonal, hexagonal, or heptagonal) and relative location on the body (e.g. ventral, dorsal, or anterior surface). The flexibility and coherence of the scales can be assessed as shown in Fig. 1(c), where half a fish was sectioned, while its integrity was retained and the scales can be flexed without apparent damage.

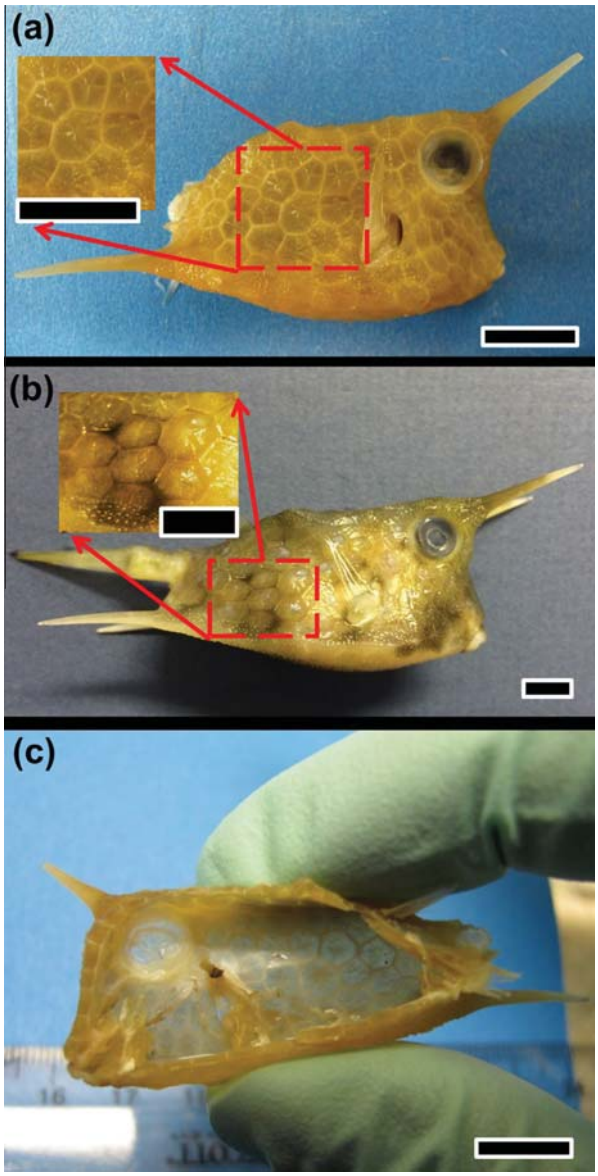

Fig. 1. The carapace of the boxfish, *Lactoria cornuta*: (a) Boxfish preserved in 1:1 isopropanol:water showing pentagonal, hexagonal, and heptagonal scutes with sizes between 3–5 mm; (b) Boxfish acquired live; note larger scutes; (c) The flexible and strong carapace under a minor simulated compression load. Scale bars: (a–c) 10 mm.

2.2. Structural characterization

The scutes were observed to be composed of a hard plate on top of a compliant base. Each of these components was evaluated to determine the relative quantities of mineral, organic, and water. Full individual scutes, separated collagen tissue (from the base of the scutes, obtained by polishing away the scutes on the surface), and highly mineralized tissue (taken from the horn [32] and assumed to be similar to the mineralized plates on the scutes) were rehydrated in saline solution for ~24 h, and tested by thermogravimetric analysis (TGA) using a SDT Q600 TGA (TA Instruments, New Castle, DE, USA) at a ramp rate of 10 °C/min and a range of 20–800 °C. This procedure has previously been reported for the determination of water, mineral, and protein in biomaterials [33]. In all cases, $N = 5$ samples were tested.

Imaging of the boxfish scutes was performed by optical microscopy (OM) using a VHX-1000 digital microscope system equipped with a CCD camera (Keyence Corporation, Osaka, Japan) and by

scanning electron microscopy (SEM) using an ultra-high resolution SEM (FEI, Hillsboro, OR, USA). Additionally, energy dispersive X-ray analysis (EDX) was performed in order to observe the chemical composition of the scutes using a Phillips XL30 environmental scanning electron microscope (ESEM) (Phillips, Portland, OR, USA). To prepare the scutes for SEM analysis, several large samples were sectioned from the carapace and immersed in a 2.5 vol.% glutaraldehyde solution for three hours in order to fix the structure, then aspirated and submerged in a graded series of ethanol solutions (30, 50, 75, 80, 95, and 100 vol.% ethanol) to further dehydrate the samples while avoiding structural damage (e.g. shrinkage or cracking of the collagen during dehydration). Finally, the samples were fractured by freezing them in liquid nitrogen, then dried using an Autosamdri-851 critical point dryer (Tousimis, Rockville, MD, USA) to remove the excess ethanol. All samples were sputter coated with iridium (Quorum Technologies Ltd., West Sussex, UK) prior to SEM observation.

Samples for micro-computed tomography (μ-CT) were prepared by wrapping the boxfish in tissues moistened with a saline solution to hydrate the structure. Macroscopic imaging of the entire boxfish body was performed by μ-CT scanning using a Skyscan 1076 μ-CT scanner (Bruker, Kontich, Belgium) with a 0.5 mm aluminum filter and scanning conditions of an isotropic voxel size of 9 μm, an electric potential of 70 peak kV (kVp), and a current of 200 μA. Microscopic imaging of the boxfish scutes was also performed by high resolution μ-CT (HR μ-CT) scanning using a Skyscan 1272 micro-CT scanner (Bruker, Kontich, Belgium) with a 0.5 mm aluminum filter and scanning conditions of an isotropic voxel size of 2 μm, an electric potential of 50 (kVp), and a current of 200 μA. In each case a post-scan beam hardening correction algorithm was applied during image reconstruction. Images and 3-D rendered models were developed using Skyscan's Dataviewer and CTVox software (Bruker, Kontich, Belgium).

2.3. Mechanical characterization

Mechanical tension, shearing and punch tests were performed on both IPA/water-preserved and fresh specimens. The IPA/water-preserved samples were partially dehydrated and had a lower water content. Before testing, these specimens remained in the IPA/water solution, while the fresh specimen samples were kept in water ~24 h prior to testing and were wrapped with a moistened tissue during preparation work of mechanical testing to retain a hydrated state during testing. These tests were performed using an Instron 3367 mechanical testing machine (Instron Corporation, Norwood, MA, USA). The tension and shear specimens were measured to be ~0.7 mm in thickness and ~2.4 mm in width at the junction between scutes. Non-active areas of the samples were glued to aluminum foil with folded edges to diminish local stress concentrations; the length of the tension samples and the width of the shear samples were measured according to the distance on the two adjacent scutes between the aluminum foil ends. Punch (penetration) test samples consisted of one active scute (surrounded by ~6–8 non-active scutes); the non-active scutes were glued to a hollow ring using a cyanoacrylate adhesive. Force was then applied with a hexagonal punch slightly smaller than the size of the active scute (area = ~3.2 mm^2) to push the scute through the orifice, placing the underlying collagen in shear and tension. All samples were imaged with SEM after mechanical testing using the sample preparation procedure described above.

3. Results and discussion

3.1. Macrostructural characterization

The entire boxfish, macroscopically imaged through μ-CT, is shown in Fig. 2 from various viewing perspectives. The carapace of the boxfish consists of numerous interlocking scutes, 3–5 mm in diameter, with the majority (~78%) of scutes being hexagonal in shape and the minority being square (~4%), pentagonal (~15%), and heptagonal (~3%). Each scute has a highly mineralized external layer and a protein base. In general, the thickness of the external mineralized layer (60–100 μm) is about 10–20% of the thickness of the whole scute. The shape and orientation of the scutes are symmetric about a centerline traced through the abdomen of the fish (Fig. 2(b)). The ventral side of the boxfish has the highest relative percentage of hexagonal scutes (85% hexagonal

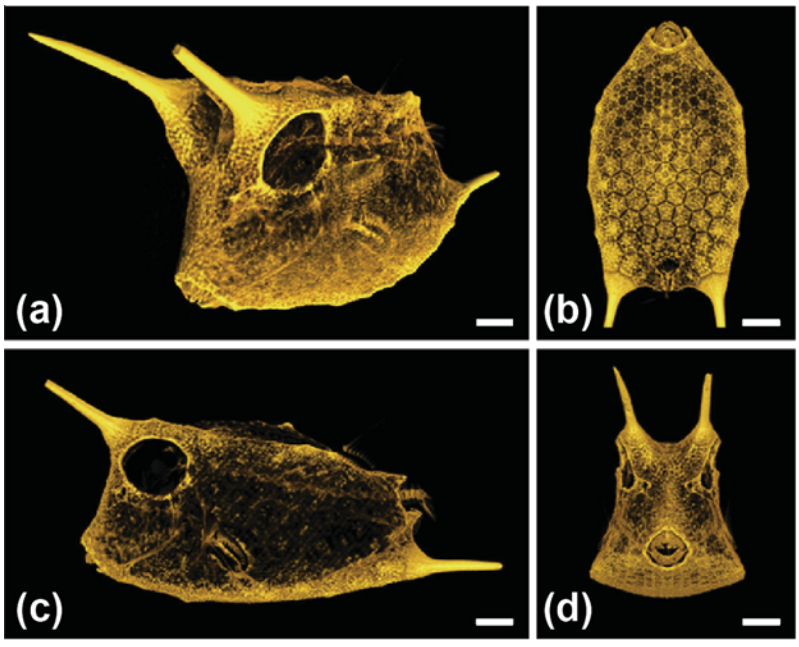

Fig. 2. Micro-computed tomography images of the boxfish: (a) Perspective view; (b) Ventral view; (c) Sinister view; (d) Anterior view. Scale bars: (a–d) 5 mm.

compared to ~75% elsewhere) resulting in the flattest surface on the carapace. The scutes at the edges of the fish body between the ventral and lateral sides (corners of the boxy shape) have the greatest curvature. On the abdomen of the fish, a low plate curvature and small suture thickness allow adjacent scutes to abut in a flattened linear fashion, while on the edges of the fish, the plates have a greater curvature, in addition to the distinctive shape changes (from hexagons to pentagons and heptagons) that allow the tessellating scutes to accommodate the overall curved, yet boxy body shape. The relative amounts of each shape of scutes are similar to previously reported results [21].

Results of the TGA experiments are shown in Table 1. The relative weight ratios of mineral to protein within the horn (~1:0.30) and collagen base (~1:12) emphasize that the scutes are designed with a rigid outer surface and very small amounts of mineral within the collagen base, indicating that the surface is similar to bone while the base is formed from lightly mineralized collagen fibrils (for comparison, the mineral/collagen weight ratio in mammalian skeletal bone is ~1:0.38 [34]).

3.2. Microstructural and material characterization

μ-CT images of an individual scute and suture connections are shown in Fig. 3, focusing on the mineralized layer. As seen in the images, a central hexagonal scute is connected to the surrounding scutes through interlocking suture interfaces (Fig. 3(a)). The raised struts on the mineralized scute face are clearly shown to be protruding from a central node (highlighted with dashed lines in Fig. 3(b)). The suture interface (shown in Fig. 3(a)) consists of "teeth" that are roughly triangular in nature and remarkably similar. If analyzed as a regular triangular wave, the suture interface has a wavelength, λ, of 65.9 ± 14.9 μm and an angle, 2θ, of 50.6 ± 9.2° (measured for all, unbroken suture teeth in Fig. 3(a), $N = 86$). Further analysis is provided in Section 4.

A SEM image of a partially polished scute along with EDX analysis is shown in Fig. 4. The scute was partially polished to expose both the external mineralized plate as well as the internal collagen base (outlined in Fig. 4(a)). Fig. 4(b)–(d) shows the distribution of carbon, calcium, and phosphorus (respectively) on the surface of the scute. The high concentration of calcium and phosphorous suggests that the external plate and the struts are mineralized. The interior structure of the scute contains collagen (high concentration of carbon) but minimal mineral (low concentration of calcium and phosphorous). These results are supported by TGA data that shows very little mineral within the collagen base.

In Fig. 5(a), the external mineralized plate was imaged with OM, then the mineralized plate was polished off and the collagen base was imaged with SEM. The inner layer of the scute is made up of two perpendicular orientations of collagen fibers that form a ladder-like structure (Fig. 5(b)) showing collagen fibers spaced at ~100 μm that are connected by numerous perpendicular collagen fibers (highlighted in Fig. 5(b)). While complex, this is not a Bouligand structure as has been previously reported for boxfish [21]. The perpendicular interface of these collagen fibers is shown at high magnification in Fig. 5(c).

SEM images of the cross section of a scute and suture are shown in Fig. 6. The observed curvature is due to differential shrinkage between and mineral and organic in the high vacuum of the SEM (The collagen shrinks, whereas the mineral dimensions remain unchanged). The two components of the scute (the highly mineralized exterior and protein base) are highlighted in Fig. 6(a). It can be seen that the collagen fibers in the base form a laminated rectangular frame (outlined as a white dashed line in Fig. 6(a)). For reference, throughout Fig. 6, this rectangular frame is highlighted. The sutured interface is magnified in Fig. 6(b) and the frame (within the bulk of the scute) is magnified in Fig. 6(c). As observed, the bulk of the collagen base is formed with the same lamellar ladder-like

Table 1
Water, protein, and mineral constituents of the entire scute, the protein component (collagen), and the mineralized tissue (the horn of the boxfish). Additionally the ratio of mineral to collagen is reported for each component. Results are weight percent (wt.%) reported as the average ± one standard deviation of $N = 5$ tests.

	Entire scute (%)	Collagen base tissue (%)	Mineralized tissue (Horn) (%)
Water	57.4 ± 3.3	67.3 ± 3.9	20.9 ± 1.7
Collagen	28.3 ± 2.2	30.2 ± 5.6	21.6 ± 0.5
Mineral	14.3 ± 3.5	2.5 ± 2.3	57.5 ± 2.0
Mineral: collagen ratio	1:2.0	1:12.2	1:0.33

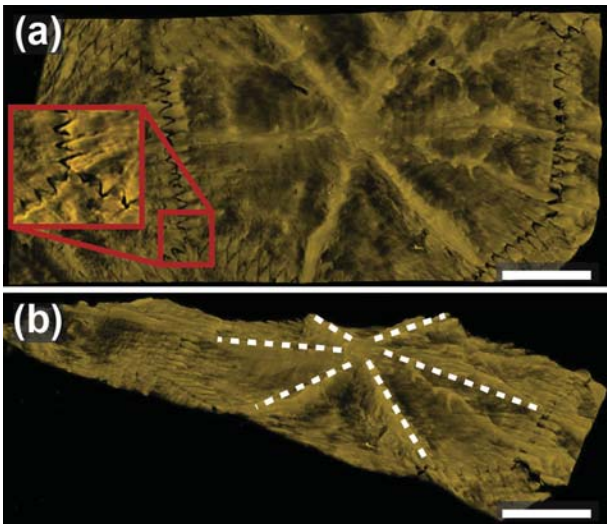

Fig. 3. High-resolution micro-computed tomography images of the boxfish scute: (a) Top view showing the interlocking hexagonal scutes and complex features of the scute body. The sutured interface is magnified; (b) Profile view showing the six raised struts (highlighted) extending from the center to the edges of the scute. Scale bars: (a–b) 500 μm.

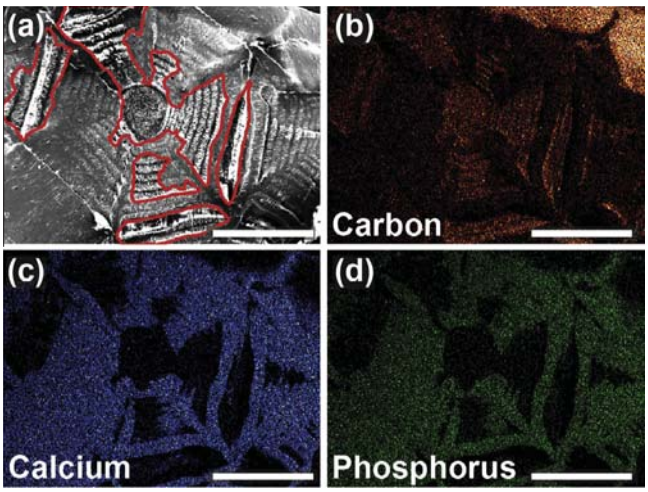

Fig. 4. Energy dispersive X-ray spectroscopy (EDX) results of a polished scute: (a) SEM micrograph of a single hexagonal scute after the external surface was partially polished to reveal the collagen base (outlined); (b–d) EDX elemental map of the same area: (b) carbon; (c) calcium; (d) phosphorus. Results show that the exterior of the scute is mineralized with calcium and phosphorous while the interior is highly non-mineralized, showing carbon. Scale bars: 1 mm.

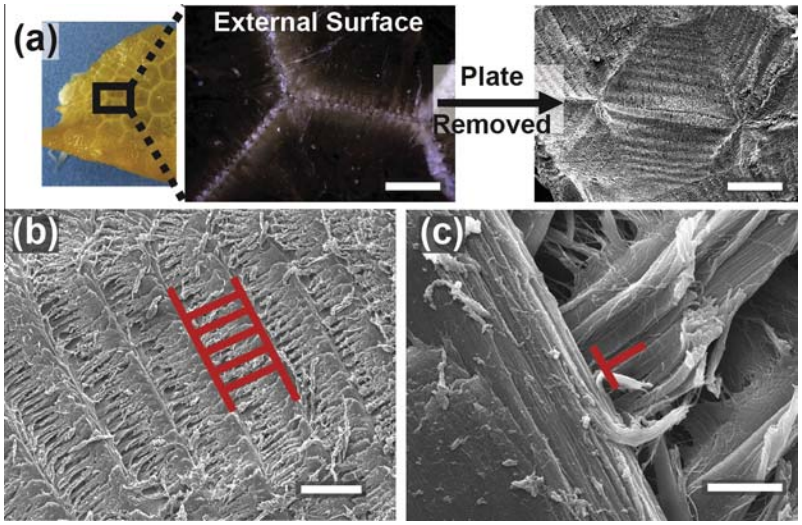

Fig. 5. Structural characterization of the scutes from the top view using SEM and optical microscopy (OM): (a) Top view of the external mineralized surface (OM) and the inner layer, with the mineralized plate removed by polishing (SEM) of the scutes and the suture interface; (b) The collagen fibers within the body of the scute showing two perpendicular orientations, giving a ladder-like appearance with steps of fibers evenly spaced; (c) High magnification view of the interface within the ladder-like collagen fiber orientations showing the perpendicular interface. Scale bars: (a) 500 μm; (b) 100 μm; (c) 5 μm.

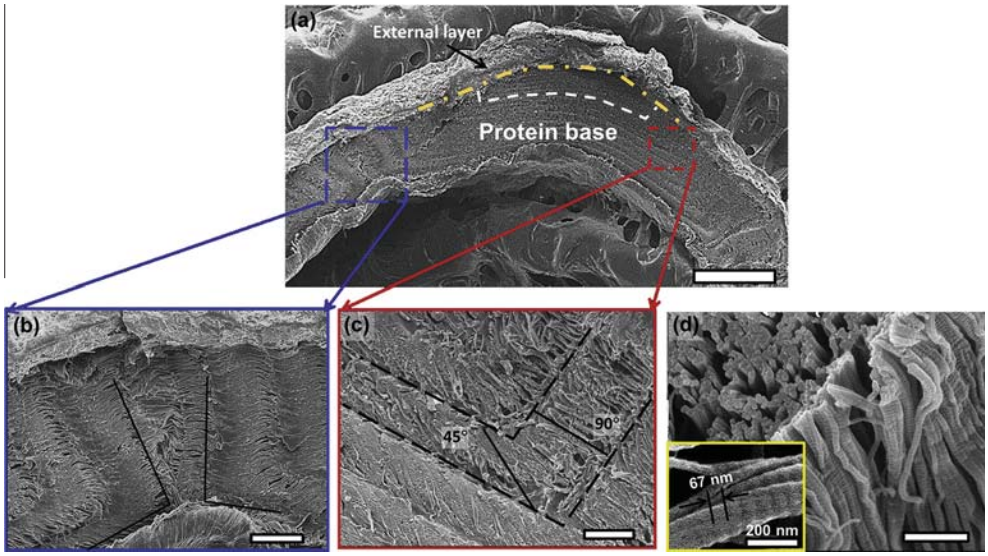

Fig. 6. Structural characterization of the cross-section of one central scute using SEM: (a) Low magnification of the scute showing the layered collagen structure in a rectangular frame orientation and highlighting the external mineralized plate and collagen base. The region is curved because of the shrinkage of collagen in the high vacuum of the SEM. The rectangular frame is examined with increasing magnification in (b–d): (b) The interface of two scutes showing the rectangular frames from each scute; (c) Corner feature of the rectangular frame layers showing the steps of the ladder-like structure changing from a perpendicular interface (90°) to a 45° interface as the frame changes orientation; (d) Collagen fibrils in the structure displaying the characteristic 67 nm spacing (in insert), note that thermogravimetric analysis demonstrated that there is little-to-no mineral within these fibers. Scale bars: (a) 500 μm; (b) 100 μm; (c) 100 μm; (d) 500 nm.

collagen fiber structure as previously shown in Fig. 5(b). The steps within the ladder-like structure are unable to maintain their perpendicular interface (90°) with the sub-frame as the ladder-like structure changes abruptly, instead rotating to approximately 45° (highlighted in Fig. 6(c)). Thus, the collagen at the boundaries between scutes has a different configuration from the lamellar structure under the scute. Finally, at high magnification, the fibrils in Fig. 6(d) show the characteristic type I collagen fibril *d*-spacing of 67 nm. A separate SEM micrograph, shown as an insert, enables the determination of $d = 67$ nm. To further illustrate the unique internal structure of the boxfish scutes, the complex dermal armor is diagramed in Fig. 7. The rectangular frame seen in the cross section (Fig. 6(a)) has been previously observed by polarized optical microscopy by Besseau and Bouligand [21]. However, the SEM appears to be considerably superior for observing the complex structural features of the organic layer.

3.3. Mechanical characterization

Representative stress–strain curves for the tension tests are shown in Fig. 8. More samples were tested but these are the most characteristic, since sliding at the grips and other spurious events limit the number of successful tests. Two conditions of the boxfish, described in Section 2, were tested in tension: partially dehydrated (preserved in 50% isopropanol) and wet. The tensile stress–strain response is characterized by a linear elastic region followed by a pseudo-plastic regime with decreasing slope. The failure is

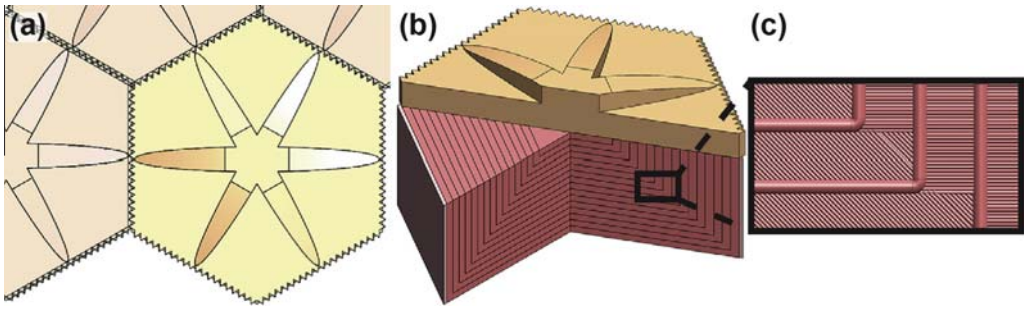

Fig. 7. Schematic diagram of the scute: (a) Top view displaying the sutured interfaces between the scutes as well as the raised struts extending from the center of the scute; (b) Cut away view displaying the top mineralized plate (gold) and collagen base (pink). The collagen base displays the distinctive rectangular frame; (c) the corner of the rectangular frame displaying a transition from the perpendicular interface to a 45° interface of the fibers within the ladder-like structure. (For interpretation of the references to color in this figure legend, the reader is referred to the web version of this article.)

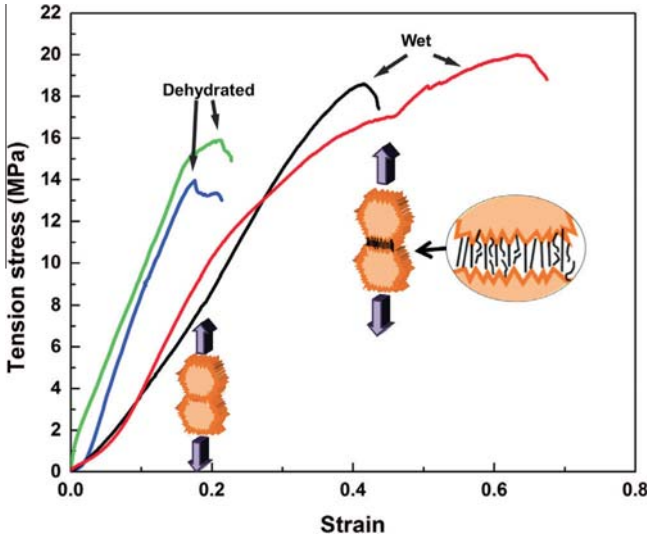

Fig. 8. Tensile stress–strain curves for dehydrated and wet conditions. Response has a linear region followed by a pseudo-plastic regime. A 'fresh' scute has lower elastic modulus, higher strength than the one preserved in isopropanol/water.

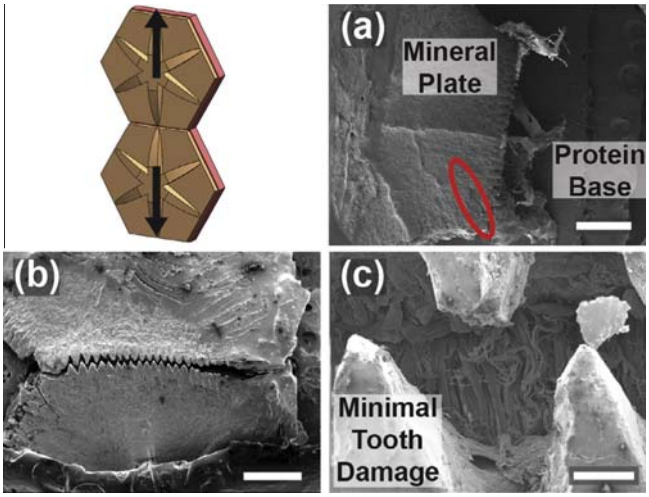

Fig. 9. SEM images of tensile sample failure in the: (a) fully fractured and (b–c) partially fractured states: (a) Low magnification of the scute after catastrophic failure showing significant collagen fiber pull-out and failure; (b) Low magnification showing the separated mineral sutures; (c) High magnification showing minimal damage to the mineralized suture teeth with significant plastic deformation and some failure to the collagen fibers. Scale bars: (a–b) 500 μm; (c) 20 μm.

accompanied by the drop in nominal stress presumably due to excessive damage accumulation.

There are definite differences between the samples preserved in IPA/water and the fresh specimens, as shown in Fig. 8. The fresh samples have a lower elastic modulus (~60 vs. 100 MPa) and a slightly higher strength (20 vs. 15 MPa) than the ones preserved in IPA/water. This is consistent with the greater presence of water in the collagen in the fresh samples, which may increase the separation between fibrils and provide additional lubrication. The mineralized scutes do not fracture; rather, failure occurs in the collagen base. As the specimens are extended, the adjacent scutes separate and the gap between them increases (shown by the sketch in Fig. 8).

After failure, the mineralized exterior plate of the scute remained relatively intact, with only minor cracking observed (highlighted in Fig. 9(a)) growing specifically from the corners of the scute. However, significant pullout is observed from the collagen base of the scute demonstrating that the majority of deformation occurs before failure in the internal collagen layers. When observing the scutes just after suture separation, low magnification (Fig. 9(b)) and high magnification (Fig. 9(c)) both show that only minor damage has occurred in the rigid suture teeth, while the collagen fibers within the suture have stretched significantly and, in some cases, began to rupture. It can be seen from Fig. 9(c) that there are no Sharpey's fibers spanning between the mineralized teeth. Sharpey's fibers are frequently observed bridging hard plates, such as in the armadillo osteoderm [6], turtle carapace [42] and cranial plates [44].

The shear tests did not provide consistent results because the response is dependent on the sequence of fracture events of the suture elements (teeth). Fig. 10 shows two separate tests on the wet specimens and two on the dehydrated ones. The shape of the curves is determined by the interaction between the teeth. Post deformation characterization of the shear specimens reveals broken teeth (Fig. 11). If the teeth slide past each other, different behaviors could also result, in addition to the formation of cracks through the teeth. In Fig. 11(b), two cracked and rotated teeth are shown. Each fracture event results in a load drop. The integrity of specimens is retained because the collagen between adjacent scutes can stretch when shear stresses are applied. The specimen will fracture only after the collagen fibers are stretched to their maximum. In contrast to tensile failure, significant deformation and fracture occurs to the mineralized suture teeth subject to shear. After suture separation (Fig. 11(a)) the suture surface is partially fractured. Even before the sutures have fully separated, significant damage to the suture teeth is apparent (Fig. 11(c); the high magnification of the box in Fig. 11(b)). Some of the collagen fibers in the fresh samples have a curled configuration, which is

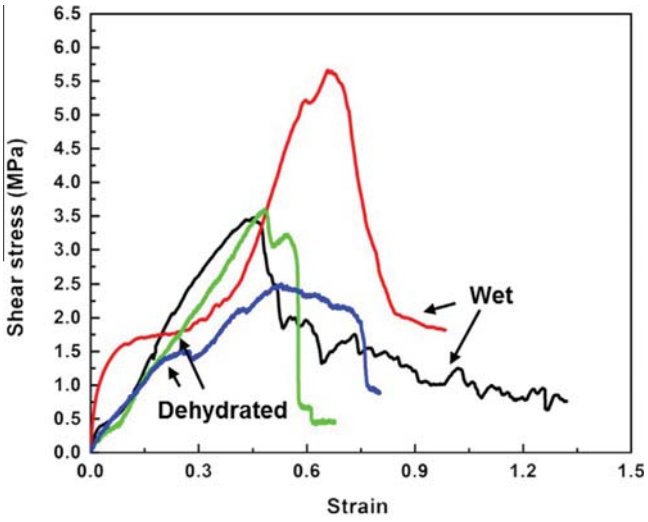

Fig. 10. Shear stress-shear strain curves for dehydrated and wet conditions. Response varies considerably from specimen to specimen because of differences in the processes of tooth fracture and collagen stretching.

assumed to be the result of pullback after failure when the stress is released (Fig. 11(d)). However, the possibility that they initially have curled configurations cannot be excluded.

The punch tests measure the resistance of the dermal layer to penetration. The punch was chosen to be flat and hexagonal such that its cross-sectional area is slightly smaller than the target punched scute. Measurements were made for the two conditions: IPA/water-preserved and fresh. The actual shape of predator teeth varies according to the species, but this flat punch satisfactorily determines the resistance of the structure to penetration. The load vs. penetration results are shown in Fig. 12. The maximum force is slightly larger for the IPA/water-preserved (85 N) than for the fresh condition (65–85 N). However, it is noted that the IPA/water-preserved scutes have smaller diameters than the fresh ones, so the IPA/water-preserved samples eventually provided a higher strength than the fresh ones. Greater flexibility of the fresh samples manifests itself by a slightly larger penetration extension at maximum load.

The load-penetration curve from the punch tests exhibits a characteristic *J*-curve, similar to that for collagen tested in tension (Fig. 8) [35]. The mechanical properties of the boxfish carapace are relatively similar to those of other collagen structures such as aligned human tendon tested in tension *in vivo* (modulus = 50 MPa, strength = 25 MPa [36,37]), which further suggests that the majority of the deformation is occurring within the collagen base of the scute and not the mineralized plate.

The surrounding (non-active) scutes after punch test failure are shown in Fig. 13(a). Similar to tensile testing, it can be seen that the suture teeth have remained relatively intact with a number of cracks forming in the surrounding scutes away from the interface. These observations suggest that, when penetrated, while there is some stress absorbed by the bulk of the scutes, the interface is significantly weaker than the mineralized plates and the majority of stress is transferred into the collagen base. The active (extracted scute) with the imprint of the punch (highlighted with a dashed line) is shown in Fig. 13(b). The ruptured fibers at the edge of the scute are shown in Fig. 13(c), demonstrating again that the fibers sheared and absorbed the majority of the plastic deformation, but the mineralized sutures remained intact. It is interesting to note that although the punch places the scute interface in shear, the stress–strain curve is not the same as the shear curve, indicating that the contributions of the mineral plates in the two testing configurations are different.

Given that in all mechanical tests the collagen fibers failed and the mineralized plates did not, the plates must be relatively fracture resistant. In brittle materials fracture toughness is increased by requiring a crack to propagate through a highly tortuous path [38,39]. Crack bridging, observed in Fig. 13(d), leaves mineral

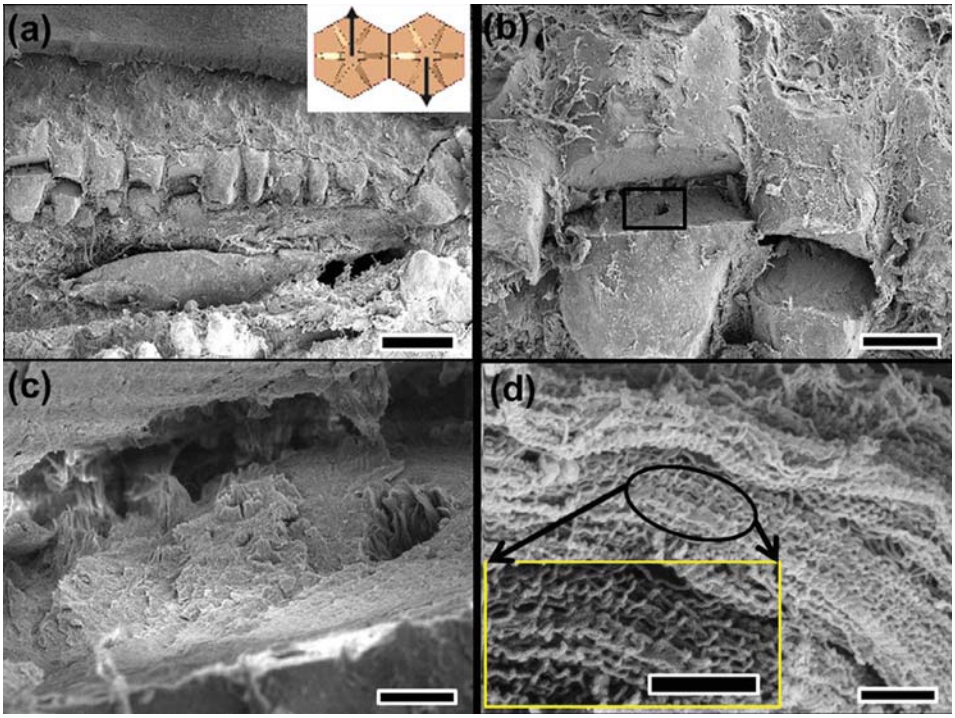

Fig. 11. SEM images of shear sample failure: (a) One side of suture with broken teeth. (b) Details of the fractured teeth; (c) collagen fibers under the scute; (d) curly collagen fibers under the scute. Scale bars: (a) 200 μm; (b) 50 μm; (c) 10 μm; (d) 1 μm.

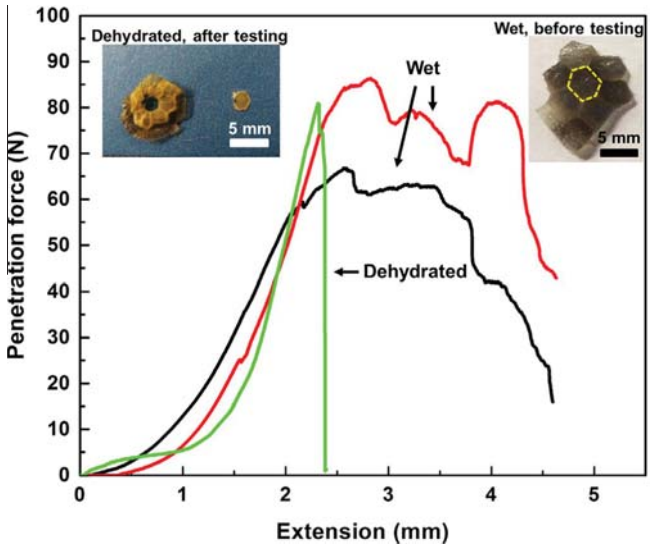

Fig. 12. Penetration tests on IPA/water-preserved and fresh (fully hydrated) specimens. Maximum loads were found to be in the range of 65–90 N. Failure is more abrupt in IPA/water-preserved specimens because of the lack of water lubrication between the collagen fibrils. In fresh specimens, failure process is gradual. Note the specimen with central scute punched out at left and outline of scute at right.

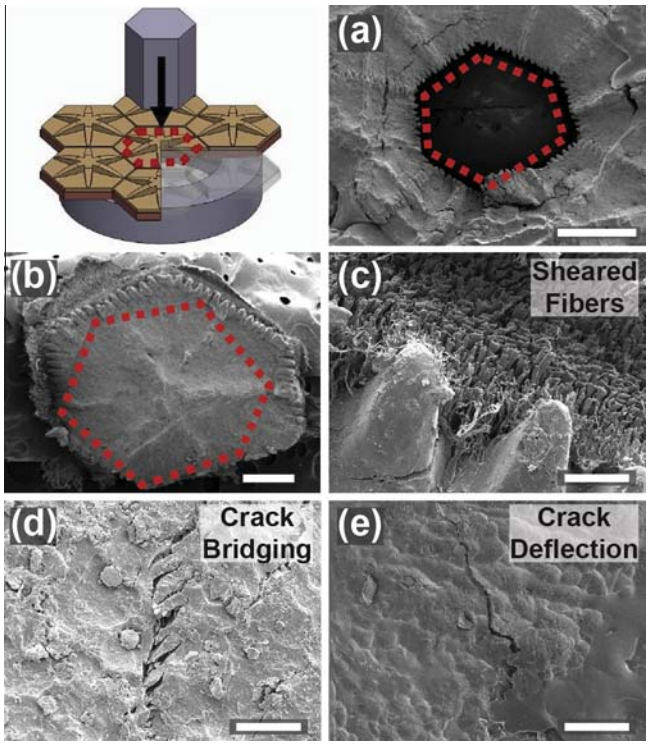

Fig. 13. SEM images of punch test failure: (a) The surrounding plates after the center active plate was punched out. The suture boundaries show a relatively clean punch out of the active scute; (b) Low magnification of the entire punched scute with the imprint of the punch highlighted; (c) Collagen fibers close to the external mineral suture showing relatively clean shearing of the fibers. Fracture mechanisms present in the mineralized plate: (d) Crack bridging; (e) Crack deflection around grains. Scale bars: (a) 1 mm; (b) 500 μm; (c) 50 μm; (d) 100 μm; (e) 50 μm.

bridges in the wake of the crack, shielding and reducing the stress at the crack tip [40]. Crack deflection, observed in Fig. 13(e), causes the crack to meander in the mineralized scute, seeking weaker interfaces and thus creating a longer and more tortuous crack path that requires more surface area to be created and higher energy for propagation. Each of these mechanisms serves to retard fracture of the mineralized plate of the scute and enable failure of the bridging collagen fibers at the interface.

4. Comparison to other dermal armors

Comparing the dermal armor of the boxfish to that in other fish highlights the unique adaptations of the boxfish carapace. The more common formation of dermal armor within fish species involves mineralized scales, which overlap and articulate in order to provide both flexibility and protection. Examples of this include ganoid scales of the alligator gar [4], longnose gar [41], and Senegal bichir [1], as well as elasmoid scales of the arapaima [10], bass [11–13], and seahorse [5], all of which have a unique configuration. In contrast, the mineralized scutes of the boxfish do not overlap and, as shown in Fig. 9(b) and (c), have little physical connectivity beyond the interdigitation of the mineralized suture interface.

While sutured interfaces are found in other organisms, the sutures of the boxfish take on a different form. The dimensions of these sutures (λ = 65.9 μm and 2θ = 50.6°) are significantly different from those reported for the triangular sutures of the red-eared slider turtle (λ = 230–400 μm, 2θ = 9.4–22°) [42], three spine stickleback fish (λ = 85–360 μm, 2θ = 6–20°) [43], and white tailed deer cranial sutures (λ = 640–2500 μm, 2θ = 9–25°) [44]; all of which have larger wavelengths and much smaller angles. In addition, these latter organisms have Sharpey's fibers that bridge the gap directly between the mineralized sutures. Li et al. [44–46] reported extensively on a mathematical model to determine the stress and failure modes of suture structures in biological systems. According to this model, the strength-optimized angle for triangular sutures made of bone- and collagen-like constituents is $2\theta = \sim 24°$ where the failure mode shifts from the compliant interface (for lower angles) to the suture teeth (for higher angles) thus producing the highest fracture strength [45]. The suture angles of the red-eared slider, stickleback, and white tailed deer are very similar to this effective suture angle and, conversely, the sutures of the boxfish are significantly larger and thus likely to create a weaker interface. In combining this with the observation that there are no Sharpey's fibers bridging between the boxfish scute sutures (Fig. 9(c)), it appears that the sutures of the boxfish are not designed for the same function as other sutures observed in nature.

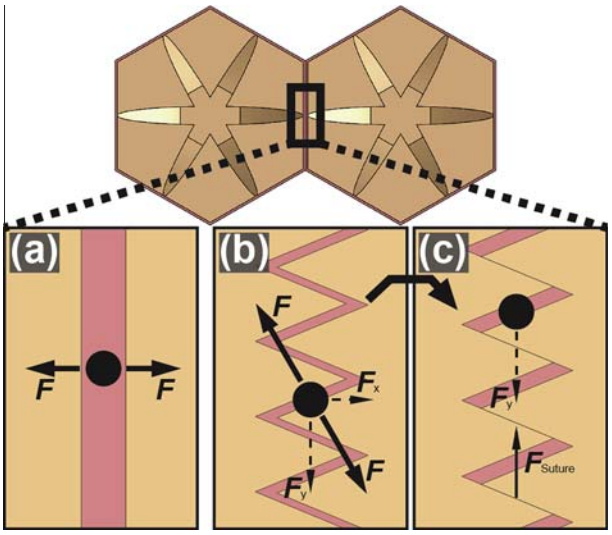

Fig. 14. Proposed mechanical advantage of sutured interface: (a) Straight interface with penetration by sharp tooth separating neighboring scutes; (b) Sutured interface with force F having tangential and normal components; (c) Tangential component of force, F_y, pushing opposite sides of teeth against each other in a locking-in mechanism.

Further separating the boxfish from other dermal armors, the ratio of mineral to protein in the scutes (1:2) is much lower than that of the seahorse (~1:0.5) [5], red seabream (1:1.2) [16], sea bass (1:1.5) [47], armadillo (~1:0.33) [6], alligator (~1:0.5) [48], and conch shell (1:0.05) [49]. This further suggests that the boxfish employs the stiff mineral component of its dermal armor in a different way from most armored organisms.

The sutures of the mineralized plates participate much more actively in the shearing mode through the sliding and fracture of teeth. However, it is also suggested that the suture configuration can also increase the bite resistance. This is shown in the schematic in Fig. 14. If a sharp tooth enters a flat interface, it will exert a force F that will separate neighboring scutes (Fig. 14(a)). On the other hand, if a suture is penetrated, the force, being normal to the surface, will have both tangential (F_y) and normal (F_x) components (Fig. 14(b)). The tangential component F_y will push the segments apart but will cause the opposing sides to decrease their gap and, if sufficient, close the gap (Fig. 14(c)). This can lead to locking-in of the scutes. Thus, this configuration is better designed to resist inter-scute penetration than a straight interface.

5. Conclusions

The carapace of the boxfish is composed of scutes with the majority (~72%) hexagonal and the minority square (~9%), pentagonal (~16%), and heptagonal (~3%) in shape. These scutes have a mineral to collagen ratio of 1:2, setting them apart from many other armored organisms where the mineral phase outweighs the collagen. The scute consists of a mineralized external surface (plate) with raised struts extending from the center toward the edges of the scute. Under this plate, collagen fibers are arranged in ladder-like structures with fibers oriented at ~90°. The cross-section of a scute reveals that these collagen structures are further oriented in a lamellar rectangular frame. While the observation of the cross-sectional rectangular frame agrees with the previous observations of Besseau and Bouligand [21], the current work demonstrates that, within this frame, the collagen structure is ladder-like, not a helicoidal, twisted-plywood configuration. The interfaces between the scutes consist of mineralized triangularly-shaped sutures arranged above bridging collagen fibers. In contrast to previously observed examples of sutures, there are no Sharpey's fibers or compliant phase bridging directly between the mineralized sutures.

Mechanical testing of the scute interface subjected to tension reveals that it is three times higher in strength and about six times higher in stiffness than in shear. In tension and penetration testing, failure occurs predominantly by stretching and failure of the collagen fibers at suture interfaces, with only minor failure within the mineralized scute. In shear, the mineralized sutures sustain more damage with extensive tooth fracture, and the final testing results depend on how many mineralized sutures fractured while they contact each other. The failure mechanism of the boxfish carapace involves inter-scute separation, shearing, and eventually, crack propagation in the scutes. This combination of damage accumulation mechanisms is effective in resisting the penetration and crushing forces by predator teeth.

Acknowledgments

We thank Prof. P. Hastings and Mr. H.J. Walker of the Scripps Institute of Oceanography, UC San Diego, for providing the boxfish specimens, Dr. James Tyler of the Smithsonian for helpful discussions, Dr. Ali Bahadur of Bruker Biospin, Billerica, MA for the high resolution μ-CT images, Mr. Ryan Anderson of CalIT2, UCSD, for help in SEM, and Dr. Esther Cory and Prof. Robert Sah of the Department of Bioengineering, UCSD, for guided analysis of the μ-CT scans, Prof. Olivia Graeve and Ms. Kyungah Seo of the Department of Mechanical and Aerospace Engineering, UCSD, for help with the TGA. This work was supported by the National Science Foundation, Division of Materials Research, Ceramics Program Grant, 1006931. We also gratefully acknowledge partial financial support from a Multi-University Research Initiative through the Air Force Office of Scientific Research (AFOSR-FA9550-15-1-0009).

Appendix A. Figures with essential color discrimination

Certain figures in this article, particularly Figs. 1–14, are difficult to interpret in black and white. The full color images can be found in the on-line version, at http://dx.doi.org/10.1016/j.actbio.2015.05.024.

References

[1] B.J.F. Bruet, J.H. Song, M.C. Boyce, C. Ortiz, Materials design principles of ancient fish armour, Nat. Mater. 7 (2008) 748–756.
[2] W. Yang, I.H. Chen, B. Gludovatz, E.A. Zimmermann, R.O. Ritchie, M.A. Meyers, Natural flexible dermal armor, Adv. Mater. 25 (2013) 31–48.
[3] W. Yang, I.H. Chen, J. McKittrick, M.A. Meyers, Flexible dermal armor in nature, JOM 64 (2012) 475–485.
[4] W. Yang, B. Gludovatz, E.A. Zimmermann, H.A. Bale, R.O. Ritchie, M.A. Meyers, Structure and fracture resistance of alligator gar (*Atractosteus spatula*) armored fish scales, Acta Biomater. 9 (2013) 5876–5889.
[5] M.M. Porter, E.E. Novitskaya, A.B. Castro-Cesena, M.A. Meyers, J. McKittrick, Highly deformable bones: unusual deformation mechanisms of seahorse armor, Acta Biomater. 9 (2013) 6763–6770.
[6] I.H. Chen, J.H. Kiang, V. Correa, M.I. Lopez, P.-Y. Chen, J. McKittrick, et al., Armadillo armor: mechanical testing and micro-structural evaluation, J. Mech. Behav. Biomed. Mater. 4 (2011) 713–722.
[7] C. Neutens, D. Adriaens, J. Christiaens, B. De Kegel, M. Dierick, R. Boistel, et al., Grasping convergent evolution in syngnathids: a unique tale of tails, J. Anat. 224 (2014) 710–723.
[8] T. Praet, D. Adriaens, S. Van Cauter, B. Masschaele, M. De Beule, B. Verhegghe, Inspiration from nature: dynamic modelling of the musculoskeletal structure of the seahorse tail, Int. J. Numer. Methods Biomed. Eng. 28 (2012) 1028–1042.
[9] M.A. Meyers, Y.S. Lin, E.A. Olevsky, P.-Y. Chen, Battle in the Amazon: arapaima versus piranha, Adv. Biomater. 14 (2012) B279–B288.
[10] Y.S. Lin, C.T. Wei, E.A. Olevsky, M.A. Meyers, Mechanical properties and the laminate structure of *Arapaima gigas* scales, J. Mech. Behav. Biomed. Mater. 4 (2011) 1145–1156.
[11] F.J. Vernerey, F. Barthelat, Skin and scales of teleost fish: simple structure but high performance and multiple functions, J. Mech. Phys. Solids 68 (2014) 66–76.
[12] D. Zhu, C.F. Ortega, R. Motamedi, L. Szewciw, F. Vernerey, F. Barthelat, Structure and mechanical performance of a "modern" fish scale, Adv. Eng. Mater. 14 (2012) B185–B194.
[13] D.J. Zhu, L. Szewciw, F. Vernerey, F. Barthelat, Puncture resistance of the scaled skin from striped bass: collective mechanisms and inspiration for new flexible armor designs, J. Mech. Behav. Biomed. Mater. 24 (2013) 30–40.
[14] T. Ikoma, H. Kobayashi, J. Tanaka, D. Walsh, S. Mann, Physical properties of type I collagen extracted from fish scales of Pagrus major and *Oreochromis niloticas*, Int. J. Biol. Macromol. 32 (2003) 199–204.
[15] A. Marino Cugno Garrano, G. La Rosa, D. Zhang, L.N. Niu, F.R. Tay, H. Majd, D. Arola, On the mechanical behavior of scales from *Cyprinus carpio*, J. Mech. Behav. Biomed. Mater. 7 (2012) 17–29.
[16] T. Ikoma, H. Kobayashi, J. Tanaka, D. Walsh, S. Mann, Microstructure, mechanical, and biomimetic properties of fish scales from *Pagrus major*, J. Struct. Biol. 142 (2003) 327–333.
[17] J.H. Song, C. Ortiz, M.C. Boyce, Threat-protection mechanics of an armored fish, J. Mech. Behav. Biomed. Mater. 4 (2011) 699–712.
[18] W. Yang, V.R. Sherman, B. Gludovatz, M. Mackey, E.A. Zimmermann, E.H. Chang, et al., Protective role of *Arapaima gigas* fish scales: structure and mechanical behavior, Acta Biomater. 10 (2014) 3599–3614.
[19] A.K. Dastjerdi, F. Barthelat, Teleost fish scales amongst the toughest collagenous materials, J. Mech. Behav. Biomed. Mater. in press. http://dx.doi.org/10.1016/j.jmbbm.2014.09.025.
[20] F.J. Meunier, H. Francillonviellot, Structure and mineralization of the scutes in ostracion lentiginosum (Teleostei, tetraodontiforme, ostraciidae), Ann. Sci. Nat. Zool. Biol. Anim. 16 (1995) 33–46.
[21] L. Besseau, Y. Bouligand, The twisted collagen network of the box-fish scutes, Tissue Cell 30 (1998) 251–260.
[22] J.C. Tyler, F. Santini, Review and reconstructions of the tetraodonitform fishes from the Eocene of Monte Bolca, Italy, with comments on related tertiary taxa, Stud. Ric. Giacimenti Terziari Bolca, Museo Civico Storia Nat. Verona 9 (2002) 47–119.

[23] F. Santini, J.C. Tyler, A phylogeny of the families of fossil and extant tetraodontiform fishes (Acanthomorpha, Tetraodontiformes), upper cretaceous to recent, Zool. J. Linnean Soc. 139 (2003) 565–617.
[24] I.K. Bartol, M. Gharib, P.W. Webb, D. Weihs, M.S. Gordon, Body-induced vortical flows: a common mechanism for self-corrective trimming control in boxfishes, J. Exp. Biol. 208 (2005) 327–344.
[25] I.K. Bartol, M. Gharib, D. Weihs, P.W. Webb, J.R. Hove, M.S. Gordon, Hydrodynamic stability of swimming in ostraciid fishes: role of the carapace in the smooth trunkfish *Lactophrys triqueter* (Teleostei: Ostraciidae), J. Exp. Biol. 206 (2003) 725–744.
[26] I.K. Bartol, M.S. Gordon, M. Gharib, J.R. Hove, P.W. Webb, D. Weihs, Flow patterns around the carapaces of rigid-bodied, multi-propulsor boxfishes (Teleostei: Ostraciidae), Integr. Comp. Biol. 42 (2002) 971–980.
[27] M. Gharib, F. Pereira, D. Dabiri, J.R. Hove, D. Modarress, Quantitative flow visualization: toward a comprehensive flow diagnostic tool, Integr. Comp. Biol. 42 (2002) 964–970.
[28] M.S. Gordon, J.R. Hove, P.W. Webb, D. Weihs, Boxfishes as unusually well-controlled autonomous underwater vehicles, Physiol. Biochem. Zool. 73 (2000) 663–671.
[29] S. Van Wassenbergh, K. van Manen, T.A. Marcroft, M.E. Alfaro, E.J. Stamhuis, Boxfish swimming paradox resolved: forces by the flow of water around the body promote manoeuvrability, J. R. Soc. Interface 12 (2014) 20141146.
[30] J.R. Hove, L.M. O'Bryan, M.S. Gordon, P.W. Webb, D. Weihs, Boxfishes (Teleostei: Ostraciidae) as a model system for fishes swimming with many fins: kinematics, J. Exp. Biol. 204 (2001) 1459–1471.
[31] P.-Y. Chen, J. Schirer, A. Simpson, R. Nay, Y.-S. Lin, W. Yang, M.I. Lopez, J. Li, E.A. Olevsky, M.A. Meyers, Predation versus protection: fish teeth and scales evaluated by nanoindentation, J. Mater. Res. 27 (2012) 100–112.
[32] W. Yang, V. Nguyen, M.M. Porter, M.A. Meyers, J. McKittrick, Structural characterization and compressive behavior of the boxfish horn, in: J. McKittrick, R. Narayan (eds.), Advances in Bioceramics and Biotechnologies II: Ceramic Transactions, 2014, pp. 105–112.
[33] L.D. Mkukuma, J.M.S. Skakle, I.R. Gibson, C.T. Imrie, R.M. Aspden, D.W.L. Hukins, Effect of the proportion of organic material in bone on thermal decomposition of bone mineral: An investigation of a variety of bones from different species using thermogravimetric analysis coupled to mass spectrometry, high-temperature X-ray diffraction, and Fourier transform infrared spectroscopy, Calcified Tissue Int. 75 (2004) 321–328.
[34] P.-Y. Chen, D. Toroian, P.A. Price, J. McKittrick, Minerals form a continuum phase in mature cancellous bone, Calcified Tissue Int. 88 (2011) 351–361.
[35] M.A. Meyers, J. McKittrick, P.-Y. Chen, Structural biological materials: critical mechanics-materials connections, Science 339 (2013) 773–779.
[36] C.N. Maganaris, J.P. Paul, In vivo human tendon mechanical properties, J. Physiol. 521 (1999) 307–313.
[37] B.H. Ji, H.J. Gao, Mechanical properties of nanostructure of biological materials, J. Mech. Phys. Solids 52 (2004) 1963–1990.
[38] R.O. Ritchie, Mechanisms of fatigue crack-propagation in metals, ceramics and composites – role of crack tip sheilding, Mater. Sci. Eng. A 103 (1988) 15–28.
[39] R.O. Ritchie, Mechanisms of fatigue-crack propagation in ductile and brittle solids, Int. J. Fract. 100 (1999) 55–83.
[40] S. Fünfschilling, T. Fett, M.J. Hoffmann, R. Oberacker, T. Schwind, J. Wippler, et al., Mechanisms of toughening in silicon nitrides: the roles of crack bridging and microstructure, Acta Mater. 59 (2011) 3978–3989.
[41] J.H. Long, M.E. Hale, M.J. McHenry, M.W. Westneat, Functions of fish skin: flexural stiffness and steady swimming of longnose gar *Lepisosteus osseus*, J. Exp. Biol. 199 (1996) 2139–2151.
[42] S. Krauss, E. Monsonego-Ornan, E. Zelzer, P. Fratzl, R. Shahar, Mechanical function of a complex three-dimensional suture joining the bony elements in the shell of the red-eared slider turtle, Adv. Mater. 21 (2009) 407–412.
[43] J.H. Song, S. Reichert, I. Kallai, D. Gazit, M. Wund, M.C. Boyce, et al., Quantitative microstructural studies of the armor of the marine threespine stickleback (*Gasterosteus aculeatus*), J. Struct. Biol. 171 (2010) 318–331.
[44] Y. Li, C. Ortiz, M.C. Boyce, A generalized mechanical model for suture interfaces of arbitrary geometry, J. Mech. Phys. Solids 61 (2013) 1144–1167.
[45] Y. Li, C. Ortiz, M.C. Boyce, Stiffness and strength of suture joints in nature, Phys. Rev. E 84 (2011) 062904.
[46] Y. Li, C. Ortiz, M.C. Boyce, Bioinspired, mechanical, deterministic fractal model for hierarchical suture joints, Phys. Rev. E 85 (2012) 031901.
[47] S. Sankar, S. Sekar, R. Mohan, S. Rani, J. Sundaraseelan, T.R. Sastry, Preparation and partial characterization of collagen sheet from fish (*Lates calcarifer*) scales, Int. J. Biol. Macromol. 42 (2008) 6–9.
[48] C.-Y. Sun, P.-Y. Chen, Structural design and mechanical behavior of alligator (Alligator mississippiensis) osteoderms, Acta Biomater. 9 (2013) 9049–9064.
[49] A.Y.M. Lin, M.A. Meyers, K.S. Vecchio, Mechanical properties and structure of *Strombus gigas*, *Tridacna gigas*, and *Haliotis rufescens* sea shells: a comparative study, Mater. Sci. Eng. C 26 (2006) 1380–1389.